

astro-ph/0005573
 SISSA 51/2000/EP
 DSF 16/2000
 May 30, 2000

Non equilibrium spectra of degenerate relic neutrinos

S. Esposito ^a, G. Miele ^a, S. Pastor ^b, M. Peloso ^b, O. Pisanti ^a

^a *Dipartimento di Scienze Fisiche
 Università di Napoli Federico II & I.N.F.N., Sezione di Napoli
 Complesso Universitario di Monte Sant'Angelo
 Via Cintia, 80126 Napoli, Italy*

^b *S.I.S.S.A. and I.N.F.N., Sezione di Trieste
 Via Beirut 2-4, 34014 Trieste, Italy*

Abstract

We calculate the exact kinetic evolution of cosmic neutrinos during the epoch previous to Big Bang Nucleosynthesis, in the case when a large neutrino asymmetry exists. By solving numerically the Boltzmann kinetic equations for the neutrino distribution functions, we find the momentum-dependent corrections to the equilibrium spectrum of neutrinos and discuss their phenomenological implications. Motivated by recent observations of the Cosmic Microwave Background Radiation, which seem to favour a larger baryon content in the Universe than that required by standard Nucleosynthesis, we also update the Nucleosynthesis bounds on neutrino chemical potentials.

1 Introduction

It is a common point of view to treat as instantaneous several (prolonged) processes that occurred in the Universe during the first instants after the Big Bang. One the most striking examples is provided by reheating after inflation. In this case, the approximation of treating all inflaton quanta as decaying at the same time $1/\Gamma$ (with Γ denoting the inflaton decay rate) is useful for many purposes, such as the computation of the reheating temperature T_R , but it may fail to reproduce the abundances of the relic particles,

especially if they have masses larger than T_R and have never been in equilibrium with the thermal bath [1].

Even when we consider the more common situation of a particle which was first in equilibrium with the radiation and then decouples, a detailed study of the whole process may provide more accurate results with respect to the standard computation, which assumes instantaneous decoupling. A particularly interesting case is that of neutrinos, which were coupled to the thermal bath via the well known weak interactions.

Let us first consider the standard situation, where neutrinos are assumed to decouple when the temperature of the primordial universe is about $2 - 3$ MeV [2], namely when the rates of the weak interactions which couple them to the electromagnetic plasma become smaller than the Hubble parameter. After this instantaneous decoupling, the neutrino spectra maintain their equilibrium shape, with the temperature redshifted as the inverse scale factor, $T_\nu \sim 1/R(t)$, due to the expansion of the Universe. In the meantime, also the temperature of the electromagnetic bath scales in the same way, until it reaches the electron mass $T_\gamma = m_e \simeq 0.5$ MeV. At this stage the $e^+ e^- \rightarrow \gamma \gamma$ annihilations occur, without affecting the relic neutrinos previously decoupled. As a consequence, the temperature of photons increases with respect to T_ν until it reaches the well-known asymptotic ratio $T_\gamma/T_\nu = (11/4)^{1/3} \simeq 1.401$.

Relaxing the assumption of instantaneous neutrino decoupling, the above results slightly modify. The main physical reason is that the neutrino plasma receives a small contribution from the $e^+ e^-$ annihilations, and its final energy density is a little bit higher than in the standard case. Neutrinos with higher momenta are more heated since, in the range of energies we are interested in, weak interactions get stronger with rising energy. This causes a momentum-dependent distortion in the neutrino spectra from the pure equilibrium Fermi–Dirac shape.

There have been a number of papers which considered the effects of non-instantaneous neutrino decoupling [3, 4, 5, 6, 7, 8, 9]. The first papers used integrated quantities to estimate that the neutrino energy density increases by a factor 1% [3, 4, 5], while subsequent works [6, 7] made some momentum-dependent calculations assuming Boltzmann statistics for neutrinos and other approximations. The full numerical computation of the evolution of the neutrino distribution functions without approximations requires the numerical solution of the Boltzmann equations, as done in [8, 9]. The most accurate results for the evolution of the neutrino distortion until complete decoupling are given in Ref. [9]. For what concerns the energy stored in the relic neutrinos, this study gives a temperature ratio after decoupling $T_\gamma/T_\nu = 1.3991$, which indeed shows that neutrinos also share a small part of the energy transfer from the $e^+ e^-$ annihilations. The method adopted in this computation has however been questioned in Ref. [10] (see also [11] for a reply to this work). One of the aims of our work is to verify the results of Ref. [9]. We have also performed a full numerical calculation, although employing a different method. Our

analysis confirms the results of Ref. [9].

The main goal of our study is to extend the previous analyses to the case in which a large asymmetry between neutrinos and antineutrinos is present. If this asymmetry is of order one, one says that neutrinos are *Fermi-degenerate*. Big Bang Nucleosynthesis (BBN) forces the baryonic asymmetry $\eta_b \equiv (n_b - n_{\bar{b}})/n_\gamma$ to be very tiny (of the order $10^{-10} - 10^{-9}$) [12], and the observed electric neutrality of the Universe translates these bounds on electrons too. However, the existence of a large asymmetry (even of order one) in the neutrino sector is an open possibility which has drawn much attention in the past.

Actually, there exist some realistic theoretical models that can generate very large values of the lepton asymmetry η_ν . From a particle physics point of view, a lepton asymmetry can be generated by an Affleck–Dine mechanism [13] without producing a large baryon asymmetry (see Refs. [14, 15, 16]), or even by active–sterile neutrino oscillations [17, 18] after the electro–weak phase transition. In general, the asymmetry is expected to be different for each neutrino family.

Important bounds on η_ν come again from BBN (see [19] for a review of non-standard BBN). The asymmetry on electronic neutrinos is the most constrained, since it has a direct influence on the weak interactions between protons and neutrons and thus affects the final ^4He abundance. Asymmetry on the neutrinos of the two other families is instead less bounded, since its only effect is to increase the expansion rate of the universe. The simultaneous presence of an asymmetry in the three neutrino families can still lead to a successful prediction of the abundances of light elements (fully degenerate BBN), provided that their values are suitably chosen. This last possibility usually requires the presence of a baryon asymmetry somewhat larger than the one allowed by standard nucleosynthesis (that is with non-degenerate neutrinos). Indeed, a high neutrino asymmetry can be considered the simplest option to save BBN predictions in case a high baryon asymmetry is required. The very recent Boomerang [20] and Maxima [21] results on the acoustic peaks of the Cosmic Microwave Background Radiation (CMBR) seem to favour [22, 23, 24, 25] high values for η_b , which may be in conflict with the bounds coming from standard BBN. In particular, in Ref. [25] it is argued that the presence of a neutrino asymmetry may contribute to both (i) improve the fits of the Boomerang data and (ii) render the high η_b needed compatible with (degenerate) BBN.

Finally, a relic neutrino asymmetry, delaying the matter domination stage, can have very significant effects on the matter power spectrum. In particular, it can suppress the power at small with respect to large scales, thus making the predictions of Cold Dark Matter models compatible with observations.

Motivated by these considerations, in this work we extend the study of non-equilibrium effects on the relic neutrino spectra to the case of non-vanishing neutrino chemical potentials (degenerate neutrinos). The paper is organized as follows. In section 2 we review the

effect of neutrino chemical potentials on BBN and other cosmological observables. The set of equations ruling the evolution of neutrino distributions and the method adopted to get the solution are presented in section 3. Numerical details are given in section 4, whereas section 5 contains our results. We discuss in section 6 some phenomenological implications of the non-equilibrium effects. Finally, in section 7 we give our conclusions.

2 Cosmological implications of degenerate neutrinos

The existence of a relic neutrino asymmetry would have important cosmological consequences mainly on Primordial Nucleosynthesis and the CMBR and matter power spectra.

Degenerate neutrinos influence BBN in two distinct ways. The first one is connected to the increase of the energy density of the primordial plasma due to a non-vanishing neutrino asymmetry. One can introduce an *effective* number of relativistic neutrinos N_ν which, for degenerate neutrinos, depends on the chemical potential of any neutrino flavour. The quantity N_ν is defined, in fact, from the total neutrino (plus antineutrino) energy density, ρ_ν , through the relation

$$\rho_\nu = N_\nu \frac{7}{4} \frac{\pi^2}{30} T_\nu^4 \quad , \quad (1)$$

which, for three massless neutrinos with chemical potentials μ_{ν_α} and in the equilibrium case, becomes

$$N_\nu = 3 + \sum_{\alpha=e,\mu,\tau} \left[\frac{15}{7} \left(\frac{\xi_\alpha}{\pi} \right)^4 + \frac{30}{7} \left(\frac{\xi_\alpha}{\pi} \right)^2 \right] \quad , \quad (2)$$

where $\xi_\alpha = \mu_{\nu_\alpha}/T_\nu$ are the degeneracy parameters. Note that N_ν does not depend on the sign of ξ_α . For what concerns BBN, $N_\nu > 3$ leads to a higher neutron to proton ratio since it favours an earlier decoupling of nucleons. This produces an increase in the final production of both ^4He (because there are more neutrons available when the nuclei form), D and ^3He (since there is less time to destroy them).

A second important effect on BBN predictions is induced by the asymmetry for ν_e only, since they directly participate in the $n \leftrightarrow p$ weak processes. An excess of electronic neutrinos over antineutrinos ($\xi_e > 0$), in fact, enhances the $n \rightarrow p$ conversion rate with respect to the inverse process, so reducing the neutron to proton ratio. In addition, the initial n/p ratio diminishes by a factor $\exp(-\xi_e)$, and this further reduces the number of neutrons available at the onset of BBN. As a consequence, the observed abundances of light elements can be achieved also in this case, but with a value of $\Omega_b h^2$ significantly higher than for $\xi_e = 0$.

When more than one neutrino species is degenerate, both the above effects combine and, as a result, one can observe particular combinations of values of ξ_α for which the

predictions of degenerate BBN are still in good agreement with the observational data on the abundances of primordial elements.

An exhaustive analysis of degenerate BBN was performed in Ref. [26] (see refs. therein for previous works), while more recently some aspects have been studied in [27, 28]. Neglecting the non-electron neutrino chemical potentials, the authors of [26] find the limits $-0.06 \leq \xi_e \leq 0.14$. Instead, for fully degenerate BBN and requiring that the Universe had a sufficiently extended period of matter domination, the neutrino degeneracy parameters lie in the wider ranges [26]

$$-0.06 \leq \xi_e \leq 1.1 \quad \text{and} \quad \begin{cases} |\xi_{\mu,\tau}| \leq 6.9 & \text{for } \xi_\mu \neq 0, \xi_\tau = 0 \text{ (or vice versa)} \\ |\xi_{\mu,\tau}| \leq 5.6 & \text{for } \xi_\mu = \xi_\tau \neq 0 \end{cases} \quad (3)$$

since, as mentioned above, at least for ${}^4\text{He}$, the effect of a positive ξ_e can be compensated by the contribution to N_ν coming from $\xi_{\mu,\tau}$.

In a very recent work [29], the BBN bounds on the neutrino degeneracies have been re-analyzed. The input parameters of degenerate BBN are ξ_e , $N_\nu(\xi_\alpha)$ and $\eta_{10} \equiv 10^{10}\eta_b$. Using an updated code, which includes all relevant physical effects that influence the ${}^4\text{He}$ abundance up to 0.1%, one can perform a likelihood analysis of compatibility between theoretical predictions and experimental data. This analysis yields contour levels which are surfaces in the three-dimensional space of these parameters. However, one should take into account other non BBN constraints for reducing the ranges of the parameters. For example, considering the upper bound on the radiation density present at recombination coming from CMBR data, ref. [30] obtains a 2σ limit $N_\nu < 13$. As far as ξ_e and η_{10} are concerned, the analysis is limited to the range $-1 \div 1$ and $1 \div 30$, respectively. The maximum for these functions is found for [29]

$$\xi_e = 0.06 \quad , \quad N_\nu = 3.45 \quad , \quad \eta_{10} = 5 \quad , \quad (4)$$

for a low value of the D abundance, and

$$\xi_e = 0.31 \quad , \quad N_\nu = 11.4 \quad , \quad \eta_{10} = 4.38 \quad , \quad (5)$$

in the high D case. We show in Figures 1 and 2 the 95% exclusion plots for the ξ_e and N_ν parameters for different values of η_{10} [29]. For low D the allowed range for η_{10} is $4.9 \div 9.6$, while for high D we have $3.8 \div 6.5$. Note that such results indicate that the recent value suggested by Boomerang data, $\eta_{10} = 10$, is only marginally consistent with degenerate BBN (an analogous result has been obtained in [31]).

Primordial nucleosynthesis is not the only framework which can be substantially affected by a non-zero relic neutrino degeneracy. For example, in the recent past, several papers have considered the imprint of this asymmetry on the power spectra of CMBR anisotropies and matter density. It has been found [32, 33, 34] that the asymmetry boosts the amplitude of the first CMBR peak, shifts the peaks to larger multipoles, and

suppresses small scale matter fluctuations (see [35] for a previous work). All these effects are the consequences of increasing the neutrino energy density, which delays the epoch of matter-radiation equality, and from their analysis one can put constraints on the neutrino degeneracy [32, 34]. Among the most recent observations, some interesting features have emerged from the new Boomerang results [20], which show a quite puzzling suppression of the second acoustic peak with respect to the first one. A possible explanation to this problem is provided by the simultaneous presence of both high baryonic and high neutrino asymmetries, as shown in Ref. [25]. The possible consequences of the neutrino degeneracy on the future CMBR measurements (Planck) are discussed in Ref. [33].

As far as the matter power spectrum is concerned, it is shown in Ref. [34] that a non-vanishing neutrino degeneracy can suppress the small scale fluctuations, so as to agree with the observations even in a pure Cold Dark Matter scenario. It is also shown in Ref. [34] that the suppression at small scales is particularly efficient if the degenerate neutrinos are massive, because free-streaming of non-relativistic neutrinos is enhanced when their average momentum is boosted by the chemical potential.

The existence of a relic lepton asymmetry enhances the contribution of massive neutrinos to the present energy content of the Universe [36, 37, 32, 34]. Actually it has been shown that even the smallest neutrino mass suggested by Super-Kamiokande data on atmospheric neutrinos [38] could be extracted from CMBR anisotropy and large-scale structure data by the future Planck satellite and Sloan Digital Sky Survey, provided that a large neutrino asymmetry exists [39].

Finally, it is worthwhile observing that there could be other implications of the presence of degenerate relic neutrinos, that include the explanation [37] of the ultra-high energy cosmic rays, beyond the Greisen-Zatsepin-Kuzmin cut-off of about 5×10^{19} eV. These cosmic rays would be produced by the protons from the annihilation of ultra-high energy neutrinos on the relic degenerate neutrinos in the galactic halo (more abundant than in the standard case) at energies close to the Z -resonance.

3 The dynamics of neutrino distributions

At the time of neutrino decoupling, the evolution of their distributions functions is described by a set of Boltzmann equations where the collisional terms are due to the weak interactions of neutrinos with the primordial plasma. Since the baryonic component is much smaller than the leptonic one, we can safely neglect its presence. In this case, the whole set of relevant reactions are those reported in Ref. [9], where a complete study of the evolution of neutrino distributions for the non-degenerate case, namely vanishing chemical potentials, is performed. In this section we describe a method which allows us to extend the results of Ref. [9] to the degenerate case.

Following the notations of Ref. [9], we choose as *time* variable $x \equiv m_e R$, and comoving momentum $y \equiv p_\nu R$, where R is the universe scale factor and m_e is the electron mass. We also define the *rescaled* photon temperature as $z \equiv T_\gamma R$.

At sufficiently high temperatures neutrinos can be considered in thermal equilibrium with the γ , e^\pm plasma through weak interactions (we always consider temperatures below the muon mass*). Thus they are described by Fermi-Dirac distributions with the same temperature of the electromagnetic plasma. However, at lower temperature one expects a different evolution for the distributions of electronic neutrinos and antineutrinos, which also experience charged current interactions due to the presence of e^\pm in the thermal bath, with respect to the neutrinos of the other families. Thus, in the following, we will assume identical distributions for muon and tau neutrinos (antineutrinos),

$$f_{\nu_\mu} = f_{\nu_\tau} \equiv f_{\nu_x}(x, y) \quad , \quad f_{\bar{\nu}_\mu} = f_{\bar{\nu}_\tau} \equiv f_{\bar{\nu}_x}(x, y) \quad , \quad (6)$$

so restricting the unknown neutrino distributions to f_{ν_e} , $f_{\bar{\nu}_e}$, f_{ν_x} and $f_{\bar{\nu}_x}$ only.

In the temperature range we are interested in, electrons and positrons are kept in thermodynamical equilibrium with photons by fast electromagnetic interactions. Thus, they are distributed according to the Fermi function [†]

$$f_{e^-}(x, y, z) = f_{e^+}(x, y, z) = \frac{1}{\exp(\sqrt{y^2 + x^2}/z) + 1} \quad . \quad (7)$$

In order to get the *time* evolution of neutrino distributions, $f_{\nu_\alpha}(x, y)$, and the rescaled photon temperature, $z(x)$, one must solve the following set of differential equations

$$\frac{d}{dx} \bar{\rho}(x) = \frac{1}{x} (\bar{\rho} - 3\bar{P})_m \quad , \quad (8)$$

$$\frac{d}{dx} f_{\nu_\alpha}(x, y) = \frac{1}{xH} I_{\nu_\alpha} [f_{\nu_e}, f_{\bar{\nu}_e}, f_{\nu_x}, f_{\bar{\nu}_x}] \quad , \quad \text{with} \quad \nu_\alpha = \nu_e, \bar{\nu}_e, \nu_x, \bar{\nu}_x \quad . \quad (9)$$

In equation (8), which states the conservation of the total energy density, $\bar{\rho}$ and \bar{P} are the dimensionless energy density and pressure of the primordial plasma, respectively,

$$\bar{\rho} = \rho \left(\frac{x}{m_e} \right)^4 \quad , \quad \bar{P} = P \left(\frac{x}{m_e} \right)^4 \quad , \quad (10)$$

and the index m in the r.h.s. reminds that only massive components in the plasma contribute. From (8), by using the expressions

$$\bar{\rho}_\gamma = \frac{\pi^2}{15} z^4 \quad , \quad (11)$$

*In the range of ξ_ν we are interested in the $\nu\bar{\nu}$ annihilation gets out of equilibrium at temperatures well below the muon mass [26, 40].

[†]We neglect the completely irrelevant e^\pm asymmetry since it is expected to be $\xi_e \sim \eta_b \leq 10^{-9}$.

$$\bar{\rho}_e = \frac{2}{\pi^2} \int_0^\infty dy y^2 \frac{\sqrt{x^2 + y^2}}{\exp(\sqrt{y^2 + x^2}/z) + 1} , \quad (12)$$

$$\bar{P}_e = \frac{2}{3\pi^2} \int_0^\infty dy \frac{y^4}{\sqrt{x^2 + y^2}} \frac{1}{\exp(\sqrt{y^2 + x^2}/z) + 1} , \quad (13)$$

$$\bar{\rho}_\nu = \frac{1}{2\pi^2} \int_0^\infty dy y^3 [f_{\nu_e}(x, y) + f_{\bar{\nu}_e}(x, y) + 2 f_{\nu_x}(x, y) + 2 f_{\bar{\nu}_x}(x, y)] , \quad (14)$$

we get the equation for the evolution of $z(x)$,

$$\frac{dz}{dx} = \frac{\frac{x}{z} F_1(x/z) - \frac{1}{4z^3} \int_0^\infty dy y^3 \left(\frac{df_{\nu_e}}{dx} + \frac{df_{\bar{\nu}_e}}{dx} + 2 \frac{df_{\nu_x}}{dx} + 2 \frac{df_{\bar{\nu}_x}}{dx} \right)}{\frac{x^2}{z^2} F_1(x/z) + F_2(x/z) + \frac{2\pi^4}{15}} , \quad (15)$$

where the functions F_i are given by

$$F_1(\tau) \equiv \int_0^\infty d\omega \omega^2 \frac{\exp(\sqrt{\omega^2 + \tau^2})}{(\exp(\sqrt{\omega^2 + \tau^2}) + 1)^2} , \quad (16)$$

$$F_2(\tau) \equiv \int_0^\infty d\omega \omega^4 \frac{\exp(\sqrt{\omega^2 + \tau^2})}{(\exp(\sqrt{\omega^2 + \tau^2}) + 1)^2} . \quad (17)$$

From eq. (15), neglecting the terms proportional to the derivative of neutrino distributions, one gets the asymptotic value $z_{eq}^D = (11/4)^{1/3}$ which represents the ratio between the photon and neutrino temperatures after the complete annihilation of e^+e^- pairs. In the presence of neutrino chemical potentials, the behaviour of $z(x)$ is in general different. However, the final value of $z(x)$ is always lower than $(11/4)^{1/3}$, showing that also the neutrino plasma is slightly heated by the e^+e^- annihilations (mathematically, this can be seen from the fact that the non-equilibrium contributions involving neutrino distributions in the r.h.s of (15) are of negative definite sign).

In the set of Boltzmann equations (9), I_{ν_α} represents the collisional integral for the single neutrino species ν_α , and is a functional of all neutrino and e^\pm distributions. At the time of neutrino decoupling, the plasma density was low enough that, in the expression of I_{ν_α} , one can safely consider only two-body weak reactions $1 + 2 \rightarrow 3 + 4$ with $\nu_\alpha \equiv 1$,

$$\begin{aligned} I_{\nu_\alpha} [f_{\nu_e}, f_{\bar{\nu}_e}, f_{\nu_x}, f_{\bar{\nu}_x}] &= \frac{1}{2 E_1} \sum_{\text{reactions}} \int \frac{d^3 p_2}{2 E_2 (2\pi)^3} \frac{d^3 p_3}{2 E_3 (2\pi)^3} \frac{d^3 p_4}{2 E_4 (2\pi)^3} \\ &\times (2\pi)^4 \delta^{(4)}(p_1 + p_2 - p_3 - p_4) F[f_1, f_2, f_3, f_4] |M_{12 \rightarrow 34}|^2 \end{aligned} \quad (18)$$

where $F \equiv f_3 f_4 (1 - f_1) (1 - f_2) - f_1 f_2 (1 - f_3) (1 - f_4)$ is the statistical factor, and $M_{12 \rightarrow 34}$ is the process amplitude. In Ref. [9] the complete list of relevant processes and corresponding squared amplitudes are reported, and it is shown that using the δ -function some of the integrals can be analytically performed, reducing I_{ν_α} to a two-dimensional integral.

In order to solve eqs. (9) and (15), instead of using a discretization in momentum space (discrete values for y , see Refs. [8, 9]), we employ a method based on orthonormal polynomials[‡]. According to this general technique, we rewrite the four unknown neutrino distribution functions as

$$f_{\nu_\alpha}(x, y) = \frac{1}{e^{y-\xi_\alpha} + 1} (1 + \delta f_{\nu_\alpha}(x, y)) \quad , \quad (19)$$

where ξ_α is the neutrino degeneracy parameter. The initial conditions on $f_{\nu_\alpha}(x, y)$ are fixed by observing that it is possible to find a starting value for the evolution parameter $x = x_{in}$, such that for temperatures larger than the corresponding T_{in} , the neutrino distributions can be safely assumed to be the equilibrium ones. This is envisaged by the Fermi factor in the r.h.s of (19), provided a vanishing δf_{ν_α} for $x = x_{in}$. In this case the initial conditions depend on the two independent input parameters ξ_e and ξ_x only, being the antineutrino equilibrium distributions characterized by the corresponding opposite chemical potentials. We take $x_{in} = m_e/(10 \text{ MeV})$ as the starting value for the evolution parameter (as in [9]). Solving the equilibrium part of eq. (15), the initial z is found to be $z_{in} = z(x_{in}) = 1.00006$.

According to (19), the function δf_{ν_α} parameterizes the departure from equilibrium and can be expanded in terms of a set of polynomials, $P_i^\alpha(y)$, as

$$\delta f_{\nu_\alpha}(x, y) = \sum_{i=0}^{\infty} a_i^\alpha(x) P_i^\alpha(y) \quad , \quad (20)$$

where $P_i^\alpha(y)$ are constructed, with the standard Gram-Schmidt orthonormalization procedure, and the requirement that they are orthonormal with respect to the Fermi function weight,

$$\int_0^\infty \frac{dy}{e^{y-\xi_\alpha} + 1} P_i^\alpha(y) P_j^\alpha(y) = \delta_{ij} \quad . \quad (21)$$

Note that each set of polynomials depends on the neutrino degeneracy parameter ξ_α through (21). By substituting (20) in eqs. (9), we can rewrite them as

$$\frac{d}{dx} a_i^\alpha(x) = \frac{1}{xH} \int_0^\infty dy_1 P_i^\alpha(y_1) I_{\nu_\alpha} [f_{\nu_e}, f_{\bar{\nu}_e}, f_{\nu_x}, f_{\bar{\nu}_x}] \quad , \quad (22)$$

with $\nu_\alpha = \nu_e, \bar{\nu}_e, \nu_x, \bar{\nu}_x$ and $i = 0, 1, \dots$. From the above considerations, the initial conditions for (22) are $a_i^\alpha(x_{in}) = 0$.

4 Numerical details

In order to solve eqs. (15) and (22), we have to truncate the infinite series in eq. (20) at a term $i = m$. The choice of m is driven by the requested accuracy, which we take to

[‡]Note that an expansion of the non-equilibrium distortions in momenta was also discussed in ref. [41]

be of the order 1% in the neutrino distortions. One can make an estimate of the error in approximating eq. (20) by comparing the results for two subsequent values m and $m + 1$. We have verified that the requested accuracy can be obtained retaining the coefficients until $m = 3$,

$$\delta f_{\nu_\alpha}(x, y) \simeq \sum_{i=0}^3 a_i^\alpha(x) P_i^\alpha(y) \quad . \quad (23)$$

If the expression of each polynomial is considered,

$$P_i^\alpha(y) = \sum_{j=0}^3 b_{ij}^\alpha y^j \quad , \quad (24)$$

one can rewrite Eq. (23) as

$$\delta f_{\nu_\alpha}(x, y) \simeq \sum_{i=0}^3 c_i^\alpha(x) y^i \quad , \quad (25)$$

where the coefficients c_i^α are given by

$$c_i^\alpha(x) = \sum_{j=0}^3 b_{ij}^\alpha a_j^\alpha(x) \quad . \quad (26)$$

The evolution equations for the $n = 4(m + 1) + 1$ unknown functions a_i^α and $z(x)$ are solved with an integrator for *stiff* equations. This is implemented in the Fortran code by calling a NAG routine for stiff equations, which uses Backward Differentiation Formulas with Newton's method and an adaptive step-size. In order to speed up the evaluation of the r.h.s. of Eq. (15), we made a fit of the functions F_1 and F_2 with a precision better than 1%. On the other side, as far as the $4(m + 1)$ equations (22) are concerned, we needed to compute the tridimensional integral on the r.h.s. of eq. (22). At this aim we used a routine implementing the Korobov-Conroy number theoretical method, repeating the integration twice for calculating the errors, and made a check on the results by comparing them with the ones obtained with other integrators.

Actually, one of the equations, that is the energy conservation law (15), is not stiff. Thus in order to check our results for some values of the neutrino chemical potentials, we used two versions of the code: in the first one we solved straightforwardly eqs. (15) and (22) as previously described, whereas in the second one we first separately considered the equilibrium component in $z(x)$, which satisfies

$$\frac{d}{dx} z_{eq} = \frac{\frac{x}{z} F_1(x/z)}{\frac{x^2}{z^2} F_1(x/z) + F_2(x/z) + \frac{2\pi^4}{15}} \quad . \quad (27)$$

In Figure 3, the quantity z_{eq} is plotted versus x . It is independent on the neutrino chemical potentials and asymptotically gives the value $z_{eq}^D = (11/4)^{1/3}$. Then, the remaining non-

equilibrium correction $\Delta z(x) \equiv z(x) - z_{eq}(x)$ satisfies the differential equation

$$\frac{d}{dx} \Delta z = \frac{-\frac{1}{4z^3} \int_0^\infty dy y^3 \left(\frac{df_{\nu_e}}{dx} + \frac{df_{\bar{\nu}_e}}{dx} + 2 \frac{df_{\nu_x}}{dx} + 2 \frac{df_{\bar{\nu}_x}}{dx} \right)}{\frac{x^2}{z^2} F_1(x/z) + F_2(x/z) + \frac{2\pi^4}{15}}, \quad (28)$$

which has a vanishing r.h.s. once the neutrinos completely decouple and their distribution functions get frozen ($df/dx = 0$). The two methods have produced very well coinciding results, and this is a check of the good performance of the NAG integrators.

5 Results

In order to compare our results with the analysis of Ref. [9], we have first solved Eqs. (15) and (22) for vanishing neutrino chemical potentials ($\xi_e = \xi_x = 0$). In Figures 4 and 5 the distortion coefficients c_i^e and c_i^x , defined in eq. (26), as a function of the *time* variable x are reported. Note that the antineutrino distributions coincide with the neutrino ones since we have vanishing chemical potentials. From the plots one can see that the coefficient evolution ends at $x \sim 10$, which means $T_\gamma = m_e z(x)/x \sim 0.07$ MeV. After this value the coefficients c_i^α reach their asymptotical values and the neutrino distributions can be well defined as *thermodynamically decoupled* from the electromagnetic plasma. Note that in both cases, the value of the coefficient c_3^α is always much smaller than the others, justifying the truncation of the expansion in (25) (in reasonable agreement with the estimate of [7]).

In Figure 6 the total distortions δf_{ν_e} and δf_{ν_x} as a function of x are reported, for three values of neutrino momentum y . Note that such distortions increase with the neutrino energy and, as expected, they are more relevant for electron neutrinos, due to the fact that only these interact with e^\pm through charge currents. This is clear from Figure 7, where we can see that the final distortion δf_{ν_α} is larger for ν_e than for ν_x and is an increasing function of neutrino energy. The contribution of the distortion to the differential energy density is given in Figure 8, where one can see that the maximum is for $y \simeq 5$. All the results obtained here for the non-degenerate case are in perfect agreement with the ones reported in [9].

In Figure 9 we plot the evolution of $\Delta z/z_{eq}$ in % with x as obtained from the solution of eq. (28) for different choices of neutrino degeneracy parameters. In all cases, it is a negative decreasing function approaching a constant value when neutrinos decouple. Thus, from this plot, one can see that the neutrinos are completely decoupled[§] (i.e. the distortions δf are frozen) at $x \simeq 3$. One also notices that Δz (the energy transfer from e^+e^- to neutrinos) slightly diminishes when the neutrino degeneracies increase. This is a

[§]Note that the *bump* at $x \sim 3 - 10$ is only due to the different values of z and z_{eq} at the late stages of their evolution, and would not appear if $z(x)$ and $z_{eq}(x)$ were plotted separately.

consequence of the fact that the rate of the e^+e^- annihilation channel into neutrinos is reduced in the presence of neutrino degeneracy.

In Figures 10 and 11 we instead report the evolution of the total distortions for all neutrino and antineutrino species as a function of x for given values of the neutrino degeneracy parameters ($\xi_e = 0.5$, $\xi_x = 1$) and for three values of neutrino momentum y . Comparing these results with the ones for the non-degenerate case, we observe that the distortions are enhanced for antineutrinos and depressed for neutrinos. The different behaviour between ν and $\bar{\nu}$ is also evident if one considers an effective Fermi distribution with a degeneracy parameter ξ_{eff} as a function of the momentum. It is easy to check that, at first order in the neutrino distortion, ξ_{eff} is given by

$$\begin{aligned}\xi_{eff}^\nu(x, y) &\simeq \xi^\nu + (1 + \exp(\xi^\nu - y))\delta f_\nu(x, y) \\ \xi_{eff}^{\bar{\nu}}(x, y) &\simeq -\xi^\nu + (1 + \exp(-\xi^\nu - y))\delta f_{\bar{\nu}}(x, y)\end{aligned}\quad (29)$$

In Figures 12 and 13 we plot the absolute values of ξ_{eff} for a fixed momentum $y = 5$. The total final distortions and their effect on the differential energy density are plotted in Figures 14 and 15. One can see from the last plot that the maxima of the neutrino distortions are displaced from $y \simeq 5$ by an approximate factor $\pm\xi_{\nu_\alpha}$.

We have solved the differential equations (15) and (22) for $0 \leq \xi_{\nu_e} \leq 0.5$ and $0 \leq \xi_{\nu_x} \leq 1$ obtaining, for all these values, the final distribution functions $f_{\nu_\alpha}^D(y)$. The general expression for this quantity as a function of the neutrino degeneracy parameters, in the above ranges, has been fitted with the following form:

$$f_{\nu_\alpha}^D(y) = \frac{1}{e^{y-\xi_\alpha} + 1} \left(1 + \sum_{i=0}^3 \sum_{j,k=0}^4 A_i^{\nu_\alpha}(j, k) \xi_e^j \xi_x^k y^i \exp \{ B_i^{\nu_\alpha} \xi_e + C_i^{\nu_\alpha} \xi_x \} \right) . \quad (30)$$

The coefficients of these fits are reported in Tables 1–5. We have checked that in order to obtain the extension of (30) for negative values of ξ_α is a good approximation to exchange the neutrino distribution functions with those of antineutrinos. An example is given in Figures 16 and 17 for the cases $\xi_x = \pm 0.6$, both calculated solving the differential equations (15) and (22).

6 Phenomenological implications of the neutrino distortions

There are two cosmological scenarios where the non-equilibrium effects on the neutrino spectra could in principle manifest: Primordial Nucleosynthesis and the spectrum of CMBR anisotropies.

We have calculated the change in the production of primordial elements when the evolution of the neutrino distortions is included. The non-equilibrium neutrino distributions produce three different effects. The first one is to increase the total energy density of the Universe during BBN and this produces a larger ${}^4\text{He}$ abundance. The inclusion of $\delta f_{\nu\alpha}$ also modifies the weak $n \leftrightarrow p$ processes, essentially increasing the rates, which has as an overall effect the destruction of some neutrons (and a smaller ${}^4\text{He}$ abundance), since they are more abundant than protons. Finally the evolution law of the photon temperature is also changed to take into account the small energy transfer from e^+e^- to neutrinos. Since the final value of the photon temperature is slightly smaller than in the standard case, this last effect leads also to a less effective production of ${}^4\text{He}$. In order to facilitate the comparison of our results with those of previous works, we have incorporated the distortions $\delta f_{\nu\alpha}(x, y)$ to the classic BBN code of Kawano [42]. We have found that the three effects of the neutrino distortions almost cancel, and the final change in the mass fraction (Y) of ${}^4\text{He}$ is only at the 10^{-4} level, in good agreement with previous analyses [8, 9, 43], which is undetectable given the current observational uncertainties. In Figure 18 we show ΔY as a function of the neutrino degeneracies (the changes in the other elements are even smaller).

The non-equilibrium effects that we have calculated will slightly modify the relic value of the neutrino energy density. We show in Figure 19 the increase of the neutrino energy density, parameterized in terms of an excess in the effective number of neutrinos N_ν as in eq. (1),

$$\rho_\nu - \rho_\nu^{eq} = \Delta N_\nu \frac{7}{4} \frac{\pi^2}{30} T_\nu^4$$

This small increase in ρ_ν can have a significant effect on the CMBR. The epoch of matter-radiation equality is very sensitive to the radiation energy density of the Universe, and the slight heating of neutrinos changes the predicted spectrum of CMBR anisotropies. Even if the effect is too small to be noticed with the present data, it has to be taken into account when determining the other cosmological parameters [44]. It has been found that the small correction to the present neutrino energy density is marginally detectable if the anisotropy and polarization of the CMBR is measured with the expected precision for the satellite mission Planck [44].

7 Conclusions

We have calculated the exact kinetic evolution of neutrinos in the early Universe until complete decoupling, extending previous analyses to the case in which a large neutrino asymmetry exists. We numerically solved the Boltzmann equations for the neutrino distribution functions, finding the momentum-dependent corrections to the equilibrium spectrum of neutrinos. At the same time, we found the final value of the ratio between

photon and neutrino temperatures, which is slightly smaller than in the standard case due to small energy transfer from the electromagnetic plasma to neutrinos due to $e^+e^- \rightarrow \nu\bar{\nu}$ processes.

Our results are in nice agreement with those of refs. [9, 11] for the non-degenerate case, obtained with a different method of solving numerically the kinetic equations. Instead of a discretization of the distribution function in momenta, we employed an expansion in momenta of the non-equilibrium part, truncated at order y^3 for an accuracy of 1%. Let us present our results for this case: $z = 1.39905$ for the final photon temperature, $\delta\rho_{\nu_e}/\rho_{\nu_e} = 0.953\%$ and $\delta\rho_{\nu_\mu}/\rho_{\nu_\mu} = 0.399\%$ for the corrections to the energy density of electron and muon/tau neutrinos, respectively.

When the neutrino degeneracies are non-zero, we found that the distortions in the neutrino and antineutrino momentum spectra are different, and larger for antineutrinos (neutrinos) for positive (negative) asymmetries. We have obtained the final distribution functions in the range of neutrino degeneracies $0 \leq \xi_{\nu_e} \leq 0.5$ and $0 \leq \xi_{\nu_x} \leq 1$, and presented the corresponding fits in Tables 1–5.

We have finally discussed two cosmological scenarios where the existence of distortions to the spectra of cosmic neutrinos could have phenomenological implications. For what concerns Primordial Nucleosynthesis, we have found that the various effects of the distortions almost cancel, leading to increases in the final mass fraction of ^4He of the order 10^{-4} with a small dependence on the neutrino degeneracies, well below the present observational uncertainties, in agreement with previous studies. Finally the distortions make a small positive contribution $\delta\rho_\nu$ to the relic value of the neutrino energy density, which slightly decreases in the presence of neutrino degeneracies. This contribution increases the radiation content of the Universe and can have an effect on the CMBR that must be taken into account when determining the other cosmological parameters [44].

Acknowledgements

The authors thank Alexander Dolgov for fruitful discussions and encouragement. S.P. was supported by the TMR network grant ERBFMRXCT960090. S.P. and M.P. were supported by I.N.F.N.

References

- [1] G. F. Giudice, E. W. Kolb and A. Riotto, hep-ph/0005123.
- [2] E. W. Kolb and M. S. Turner, *The Early Universe*, (Addison-Wesley, 1990).

- [3] D.A. Dicus, E.W. Kolb, A.M. Gleeson, E.C. Sudarshan, V.L. Teplitz and M.S. Turner, Phys. Rev. **D26** (1982) 2694.
- [4] M.A. Herrera and S. Hacyan, Astrophys. J. **336** (1989) 539.
- [5] N.C. Rana and B. Mitra, Phys. Rev. **D44** (1991) 393.
- [6] S. Dodelson and M.S. Turner, Phys. Rev. **D46** (1992) 3372.
- [7] A.D. Dolgov and M. Fukugita, Phys. Rev. **D46** (1992) 5378.
- [8] S. Hannestad and J. Madsen, Phys. Rev. **D52** (1995) 1764.
- [9] A.D. Dolgov, S.H. Hansen, and D.V. Semikoz, Nucl. Phys. **B503** (1997) 426.
- [10] N.Y. Gnedin and O.Y. Gnedin, Astrophys. J. **509** (1998) 11.
- [11] A.D. Dolgov, S.H. Hansen, and D.V. Semikoz, Nucl. Phys. **543** (1999) 269.
- [12] K.A. Olive, G. Steigman and T.P. Walker, Phys. Rep. (2000), in press [astro-ph/9905320].
- [13] I. Affleck and M. Dine, Nucl. Phys. **B249** (1985) 361.
- [14] A. Casas, W.Y. Cheng and G. Gelmini, Nucl. Phys. **B538** (1999) 297.
- [15] J. March-Russell, H. Murayama and A. Riotto, J. High Energy Phys. **11** (1999) 015.
- [16] J. McDonald, Phys. Rev. Lett. **84** (2000) 4798.
- [17] R. Foot, M.J. Thomson and R.R. Volkas, Phys. Rev. **D53** (1996) 5349.
- [18] A.D. Dolgov, S.H. Hansen, S. Pastor and D.V. Semikoz, Astropart. Phys. (2000), in press [hep-ph/9910444].
- [19] S. Sarkar, Rept. Prog. Phys. **59** (1996) 1493.
- [20] P. de Bernardis *et al.*, Nature **404** (2000) 955.
- [21] A. Balbi *et al.*, astro-ph/0005124.
- [22] M. White, D. Scott and E. Pierpaoli, astro-ph/0004385.
- [23] A.E. Lange *et al.*, astro-ph/0005004.
- [24] S.H. Hansen and F.L. Villante, astro-ph/0005114.
- [25] J. Lesgourgues and M. Peloso, astro-ph/0004412.
- [26] H. Kang and G. Steigman, Nucl. Phys. **B372** (1992) 494.

- [27] K. Kohri, M. Kawasaki and K. Sato, *Astrophys. J.* **490** (1997) 72.
- [28] S.E. Whitmire and R.J. Scherrer, *Phys. Rev.* **D61** (2000) 083508.
- [29] S. Esposito, G. Mangano, G. Miele and O. Pisanti, astro-ph/0005571.
- [30] S. Hannestad, astro-ph/0005018.
- [31] M. Orito, T. Kajino, G.J. Mathews, and R.N. Boyd, astro-ph/0005446.
- [32] J.A. Adams and S. Sarkar, preprint OUTP-98-70P and talk presented at the workshop on *The Physics of Relic Neutrinos*, Trieste, September 1998.
- [33] W.H. Kinney and A. Riotto, *Phys. Rev. Lett.* **83** (1999) 3366.
- [34] J. Lesgourgues and S. Pastor, *Phys. Rev.* **D60** (1999) 103521.
- [35] G.B. Larsen and J. Madsen, *Phys. Rev.* **D52** (1995) 4282.
- [36] P.B. Pal and K. Kar, *Phys. Lett.* **B451** (1999) 136.
- [37] G. Gelmini and A. Kusenko, *Phys. Rev. Lett.* **82** (1999) 5202.
- [38] Y. Fukuda *et al.* [Super-Kamiokande Collaboration], *Phys. Rev. Lett.* **81** (1998) 1562.
- [39] J. Lesgourgues, S. Pastor and S. Prunet, *Phys. Rev. D* (2000), in press [hep-ph/9912363].
- [40] K. Freese, E.W. Kolb and M.S. Turner, *Phys. Rev.* **D27** (1983) 1689.
- [41] A. D. Dolgov, *Nucl. Phys.* **B496** (1997) 437.
- [42] L. Kawano, Report FERMILAB-PUB-92-04-A.
- [43] B.D. Fields, S. Dodelson and M.S. Turner, *Phys. Rev.* **D47** (1993) 4309.
- [44] R.E. Lopez, S. Dodelson, A. Heckler and M.S. Turner, *Phys. Rev. Lett.* **82** (1999) 3952.

j	k	$i = 0$	$i = 1$	$i = 2$	$i = 3$
0	0	-0.02553	-0.02742	0.0613	-0.00148
0	1	-0.03074	0.09055	0.1187	-0.00385
0	2	-0.02399	-0.12646	0.1148	-0.00271
0	3	0.00993	0.08959	0.0496	-0.00505
0	4	-0.00835	-0.02629	0.0500	-0.00240
1	0	0.15567	-0.26435	0.3008	-0.00832
1	1	0.17914	0.94075	0.0113	0.02173
1	2	0.18841	1.6935	3.0263	-0.21256
1	3	-0.11087	1.5932	-2.8577	0.24631
1	4	0.02723	-0.58620	1.4382	-0.13254
2	0	-0.40884	-1.4464	1.1112	-0.03258
2	1	-0.44811	2.4330	11.350	-0.74164
2	2	-0.58457	1.9514	-41.698	3.1148
2	3	0.14559	-6.3494	64.550	-4.9244
2	4	0.29394	3.3575	-27.901	2.2084
3	0	0.53673	0.88730	-0.4563	0.01508
3	1	0.60942	1.6758	-38.547	2.9535
3	2	0.58380	-15.225	190.83	-15.036
3	3	0.86444	23.582	-295.87	24.047
3	4	-1.5265	-10.938	141.24	-11.816
4	0	-0.28813	-8.3610	5.7948	-0.20675
4	1	-0.38332	19.873	53.972	-3.9248
4	2	-0.38332	-14.305	-208.88	17.168
4	3	-1.5869	-1.7584	351.64	-29.033
4	4	1.7923	4.1868	-163.85	13.631

Table 1: Values of the coefficients $10^2 \cdot A_i^{\nu_e}(j, k)$.

j	k	$i = 0$	$i = 1$	$i = 2$	$i = 3$
0	0	-0.02583	-0.0270	0.0612	-0.001473
0	1	-0.07963	-0.0925	-0.13583	-0.003438
0	2	-0.19747	-0.1836	0.13921	-0.006921
0	3	0.10388	-0.0596	-0.07767	0.002688
0	4	-0.38097	-0.2018	0.01913	-0.007743
1	0	0.1593	0.0815	-0.00312	0.005457
1	1	0.55275	2.8083	-0.07579	0.006372
1	2	0.72928	-17.257	0.36785	0.077571
1	3	0.02571	35.200	-0.52872	-0.12317
1	4	2.0129	-19.508	0.23881	0.098611
2	0	-0.42554	0.4269	-0.03213	-0.008874
2	1	-1.9241	-34.408	0.93314	0.017523
2	2	2.0039	253.21	-4.0506	-0.39445
2	3	-7.1596	-508.30	5.7437	0.81968
2	4	-1.1437	310.97	-2.5930	-0.55169
3	0	0.58393	0.6891	0.07955	0.007278
3	1	3.7370	130.57	-0.02633	-0.053902
3	2	-12.534	-923.56	11.969	0.77523
3	3	28.494	1889.8	-17.361	-1.8111
3	4	-9.6482	-1133.0	7.9446	1.2011
4	0	-0.33342	1.7667	-0.06659	-0.002354
4	1	-2.9576	-137.06	2.3217	0.034407
4	2	14.374	1057.1	-10.975	-0.50053
4	3	-30.386	-2145.0	16.238	1.2960
4	4	13.947	1323.8	-7.5198	-0.87897

Table 2: Values of the coefficients $10^2 \cdot A_t^{\bar{p}_e}(j, k)$.

j	k	$i = 0$	$i = 1$	$i = 2$	$i = 3$
0	0	-0.02048	-0.0226	0.03145	-0.00113
0	1	-0.00816	-0.121	0.07636	-0.00360
0	2	0.02952	-0.1641	0.08906	-0.00585
0	3	-0.01427	-0.0915	0.0388	-0.00121
0	4	0.00164	-0.1115	0.06871	-0.00862
1	0	0.10202	-0.1019	-0.05819	0.00520
1	1	0.01809	-0.1574	-0.13567	0.01819
1	2	-0.03122	-1.7927	-0.26456	0.01774
1	3	-0.10827	0.1559	0.17303	0.02818
1	4	0.07637	-0.2702	-0.26288	0.02266
2	0	-0.23508	-0.1848	0.04808	-0.01103
2	1	0.10452	-7.3509	0.20488	-0.05013
2	2	-0.72088	18.548	0.58328	0.02313
2	3	1.4737	-21.042	-1.3891	-0.21736
2	4	-0.74609	31.385	0.94944	0.07007
3	0	0.28818	-0.4307	-0.00637	0.01223
3	1	-0.42478	24.659	-0.78479	0.09185
3	2	2.5423	-95.411	0.94741	-0.20551
3	3	-4.3721	109.17	0.56259	0.67354
3	4	2.1039	-36.302	-0.64878	-0.38348
4	0	-0.15066	-0.4019	-0.01961	-0.00563
4	1	0.40797	-32.973	1.0519	-0.07554
4	2	-2.3936	97.440	-2.6746	0.25515
4	3	3.9369	-127.23	2.1778	-0.67542
4	4	-1.8635	36.555	-0.80063	0.42456

Table 3: Values of the coefficients $10^2 \cdot A_i^{\nu_x}(j, k)$.

j	k	$i = 0$	$i = 1$	$i = 2$	$i = 3$
0	0	-0.02042	-0.0226	0.0315	-0.00113
0	1	0.01559	0.0401	0.071	-0.00421
0	2	0.02578	0.1409	0.079	-0.00977
0	3	0.00504	0.0229	0.0326	-0.00147
0	4	-0.00042	0.1407	0.0444	-0.01848
1	0	0.15327	-0.1203	0.1222	0.00205
1	1	-0.11371	1.325	-0.0573	0.00577
1	2	-0.19499	-5.7122	1.9867	0.04055
1	3	-0.06009	11.340	-2.3154	-0.06816
1	4	0.02246	-5.3401	1.2701	0.08527
2	0	-0.49132	-0.8147	0.2621	-0.0016
2	1	0.33071	-14.744	6.0747	-0.02339
2	2	0.67541	100.37	-28.004	0.01113
2	3	0.24575	-164.39	45.705	0.11598
2	4	-0.13844	95.594	-21.9132	-0.17379
3	0	0.76303	1.1339	0.1916	-0.00013
3	1	-0.43814	62.116	-22.855	0.15731
3	2	-1.1622	-390.91	124.88	-0.75599
3	3	-0.45742	662.84	-202.18	1.0609
3	4	0.32338	-373.06	102.07	-0.4143
4	0	-0.46614	-5.7445	0.6584	0.00111
4	1	0.21885	-6.2130	28.568	-0.22558
4	2	0.77295	480.42	-143.87	1.23273
4	3	0.34072	-752.91	240.49	-2.0296
4	4	-0.26958	458.28	-120.81	1.0202

Table 4: Values of the coefficients $10^2 \cdot A_i^{\bar{p}_x}(j, k)$.

ν_α	i	$B_i^{\nu_\alpha}$	$C_i^{\nu_\alpha}$
ν_e	0	7.447	-1.268
ν_e	1	-4.521	2.781
ν_e	2	-5.129	-2.015
ν_e	3	-5.405	-2.514
$\bar{\nu}_e$	0	5.011	-3.179
$\bar{\nu}_e$	1	-3.079	-3.144
$\bar{\nu}_e$	2	0.0847	2.287
$\bar{\nu}_e$	3	3.353	-2.473
ν_x	0	5.07	0.7437
ν_x	1	-4.445	-1.975
ν_x	2	1.858	-2.301
ν_x	3	4.689	-2.862
$\bar{\nu}_x$	0	8.037	-0.3521
$\bar{\nu}_x$	1	-6.341	-1.438
$\bar{\nu}_x$	2	-3.938	-2.365
$\bar{\nu}_x$	3	1.812	-4.078

Table 5: Values of the coefficients $B_i^{\nu_\alpha}$ and $C_i^{\nu_\alpha}$.

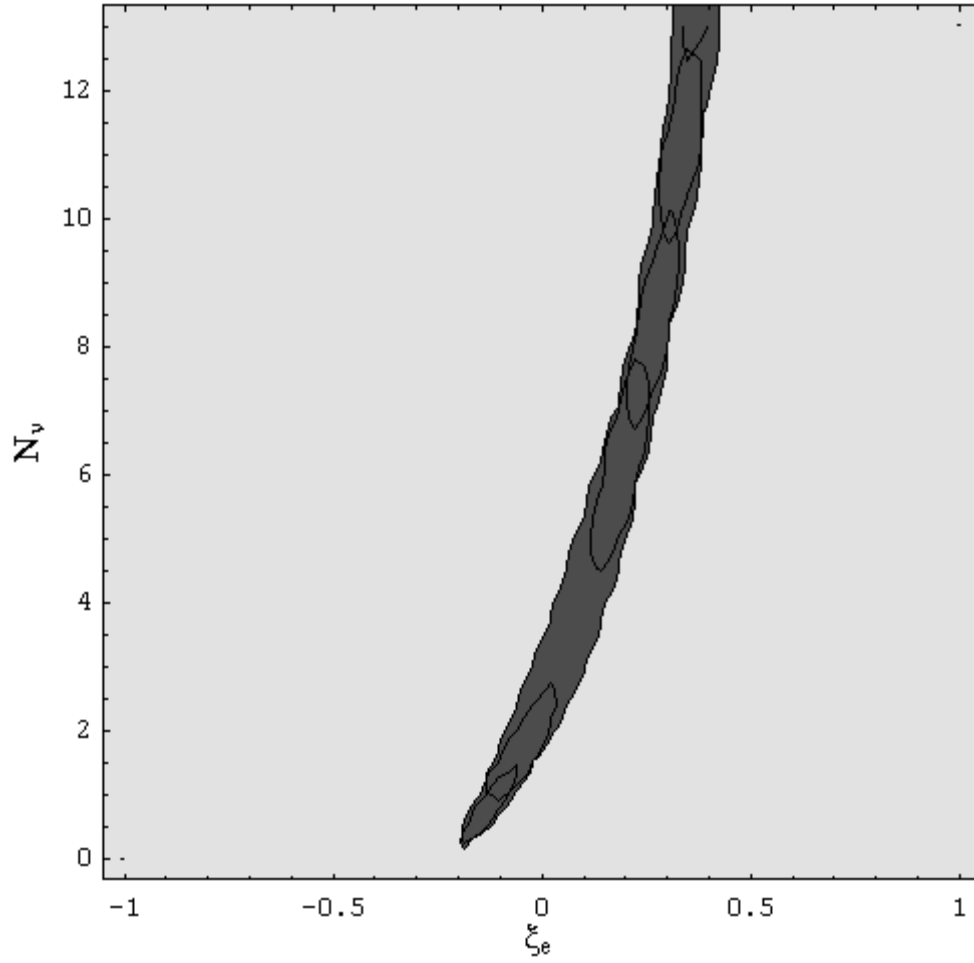


Figure 1: The 95% exclusion plot for the variables $\xi_e - N_\nu$ for low D experimental value [29]. The dark area represents the BBN allowed region. From bottom left to top right the contours in solid correspond to increasing values for η_{10} in the range $4.9 \div 9.6$.

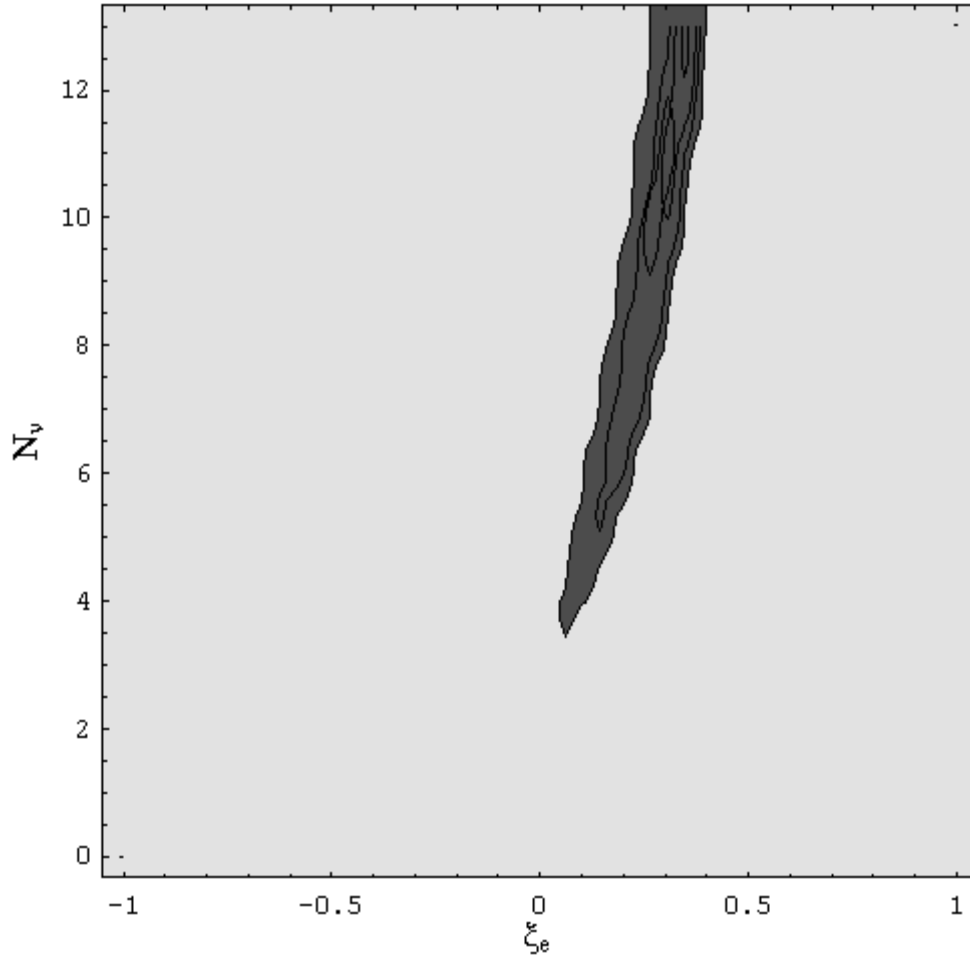


Figure 2: The 95% exclusion plot for the variables $\xi_e - N_\nu$ for high D experimental value [29]. The dark area represents the BBN allowed region. From bottom left to top right the contours in solid correspond to increasing values for η_{10} in the range $3.8 \div 6.5$.

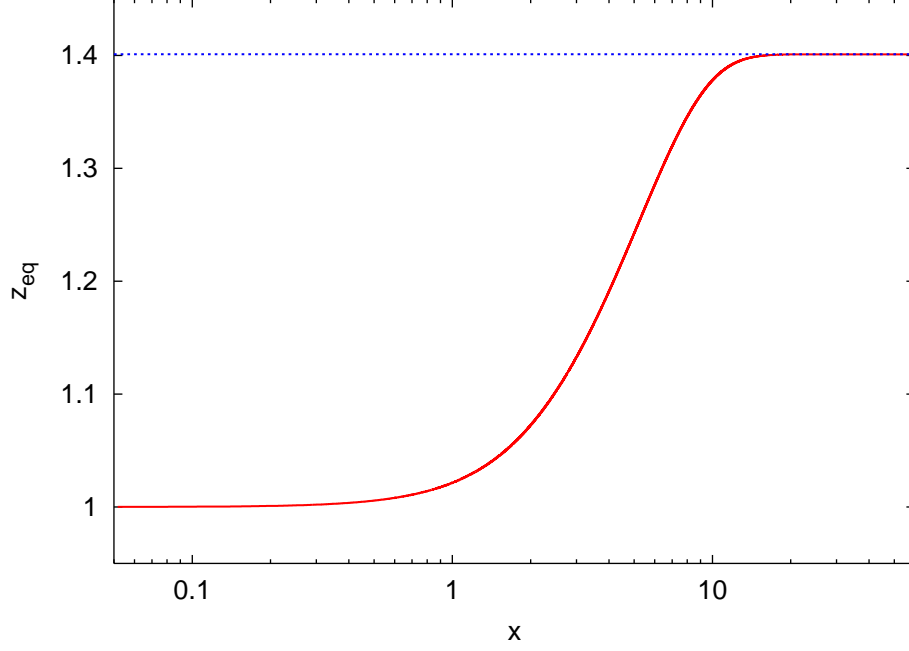


Figure 3: Evolution of the quantity $z_{eq}(x)$, defined in eq. (27). The asymptotical value represents the well-known value $z_{eq}^D = (11/4)^{1/3}$.

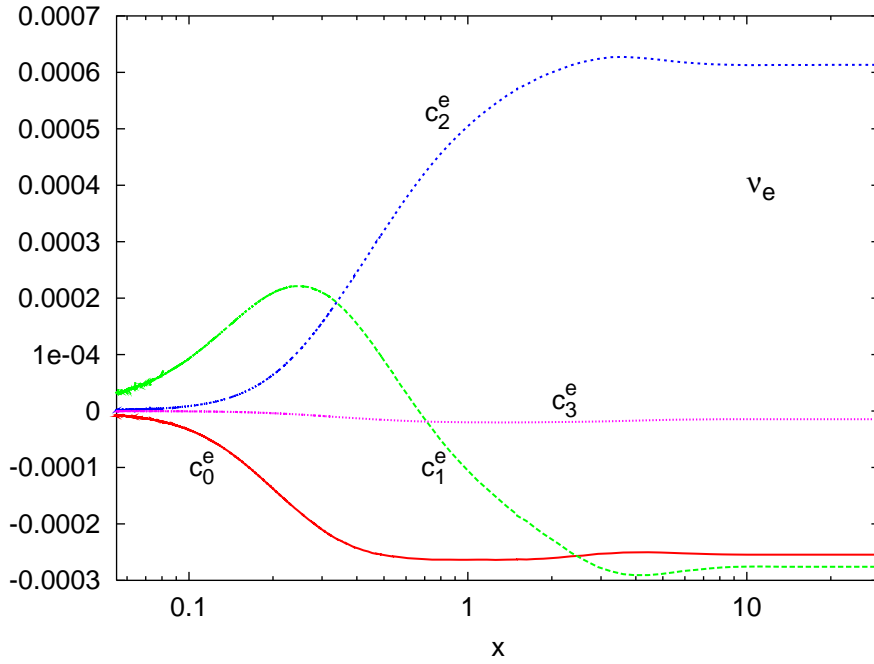


Figure 4: Evolution of the coefficients c_i^e , as a function of x (non-degenerate case).

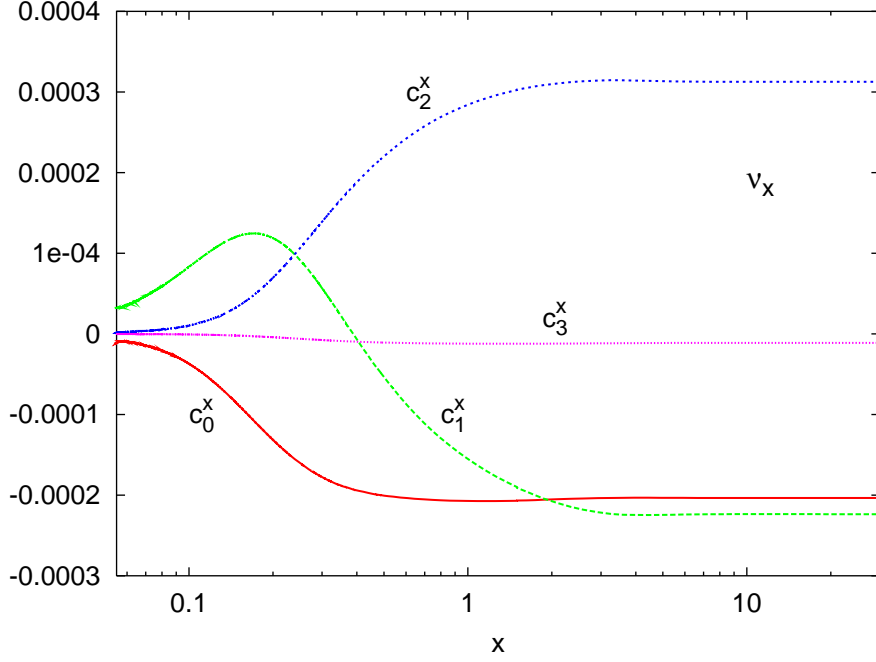


Figure 5: Same as previous figure, for c_i^x .

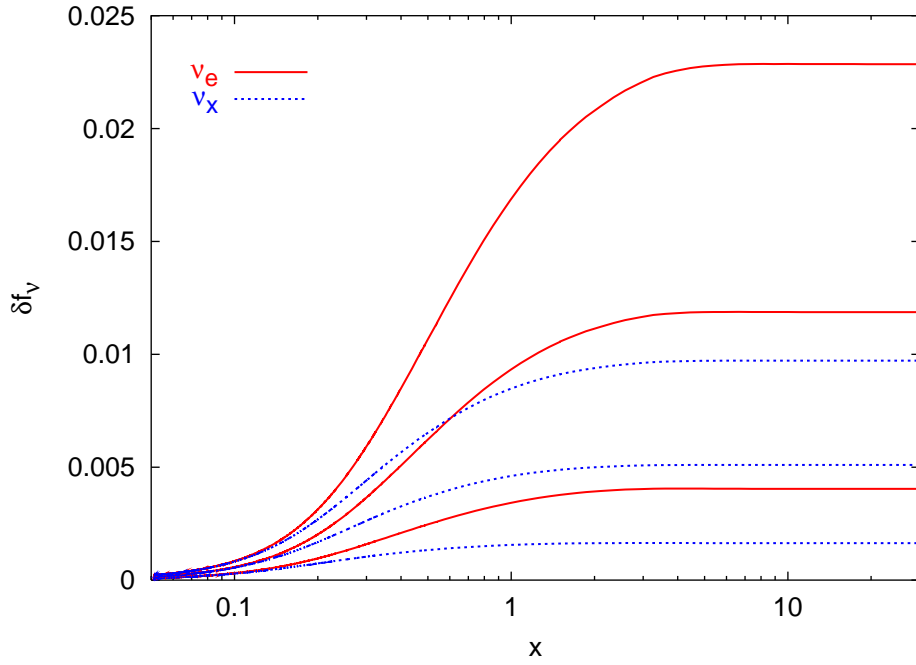


Figure 6: The evolution of the total distortion δf_{ν_α} (25), as a function of x (non-degenerate case) for three values of neutrino momentum y . From bottom to top: $y = 3$, $y = 5$ and $y = 7$.

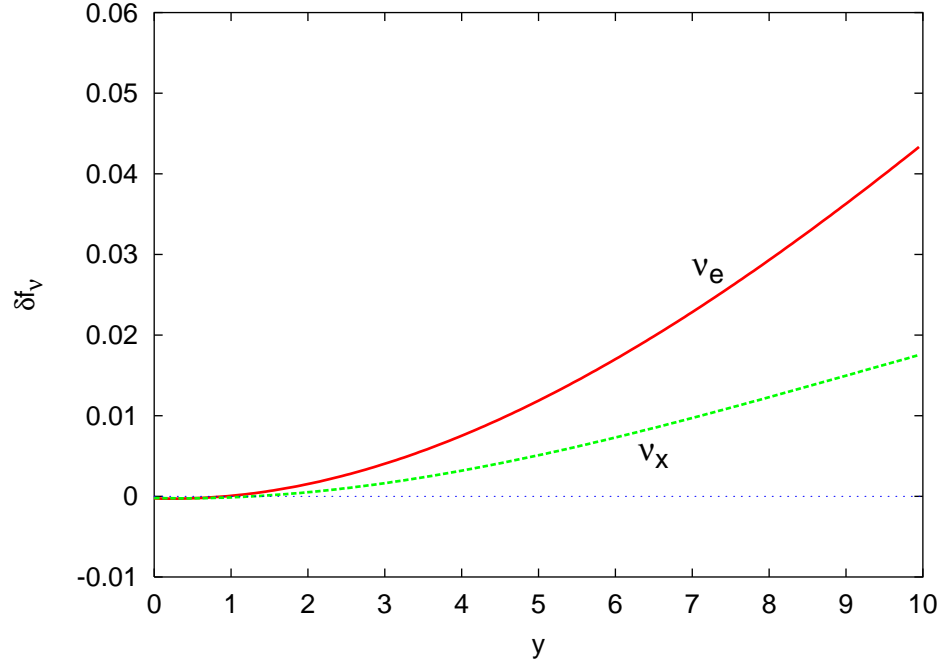


Figure 7: The final distortion as a function of momentum for the non-degenerate case.

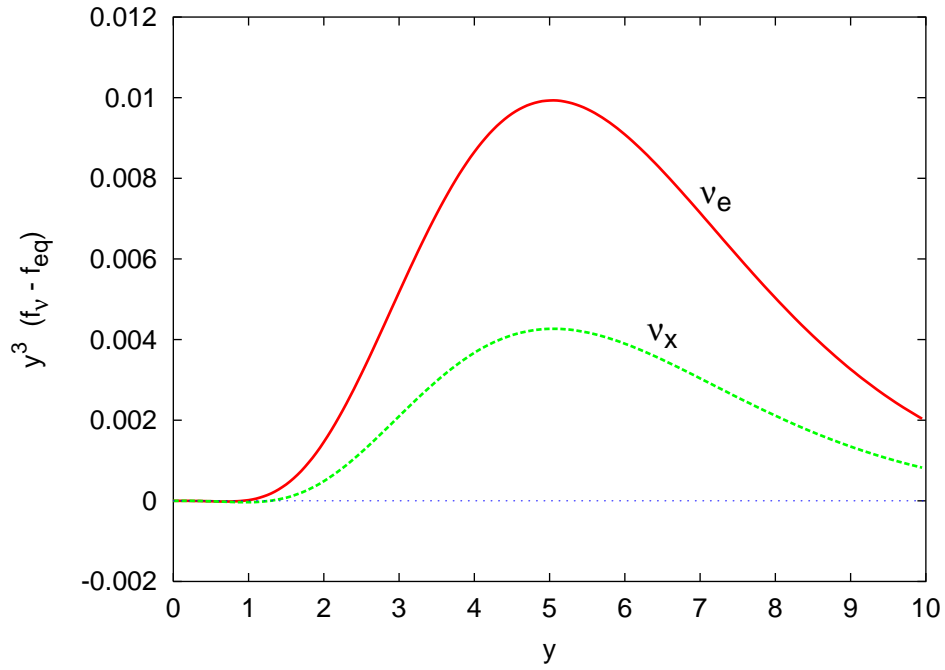


Figure 8: Final distortion of the differential energy density, as a function of momentum (non-degenerate case).

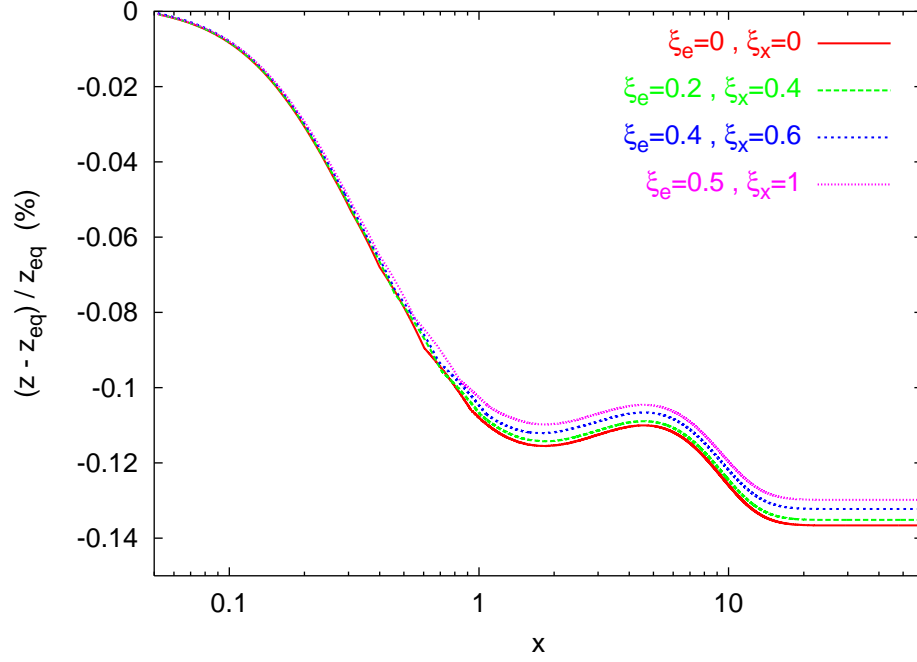


Figure 9: The evolution of $\Delta z/z_{eq}$ from eqs. (27) and (28), as a function of x for four choices of the neutrino degeneracy parameters ξ_e , ξ_x .

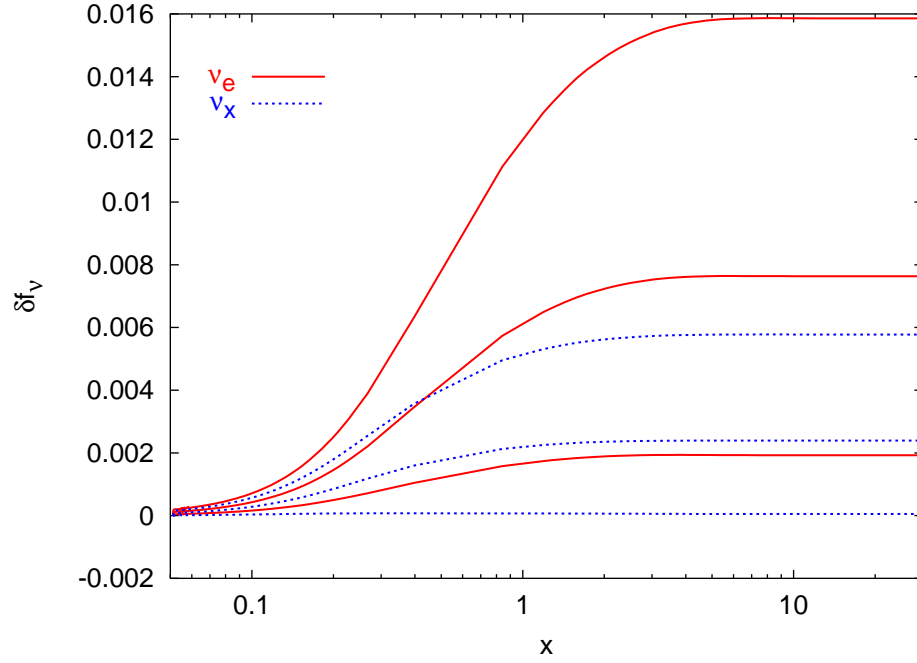


Figure 10: The evolution of the total distortion δf_{ν_α} , as a function of x ($\xi_e = 0.5$, $\xi_x = 1$) for three values of neutrino momentum y . From bottom to top: $y = 3$, $y = 5$ and $y = 7$.

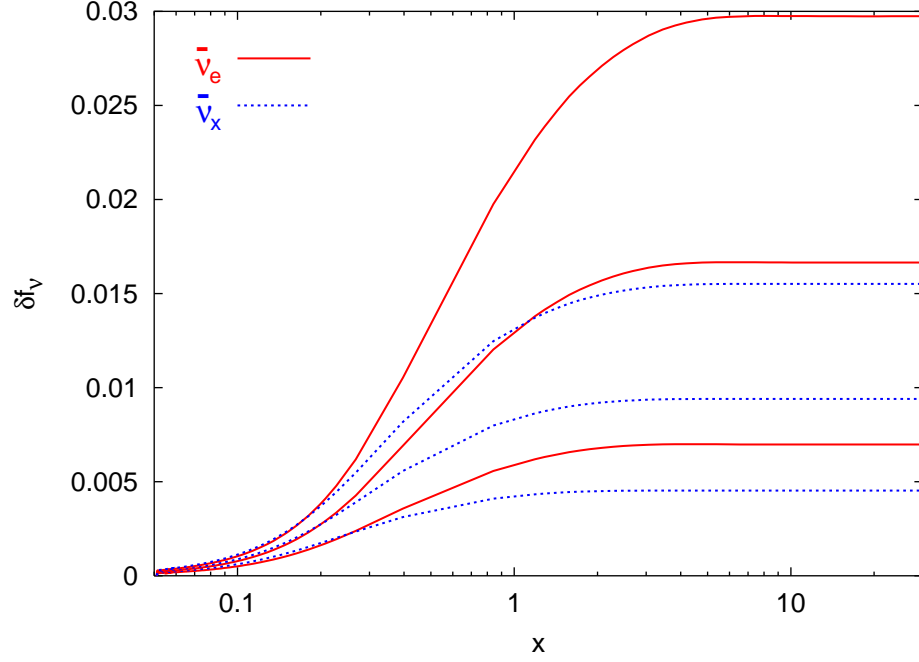


Figure 11: Same as previous figure, for the antineutrino distortions.

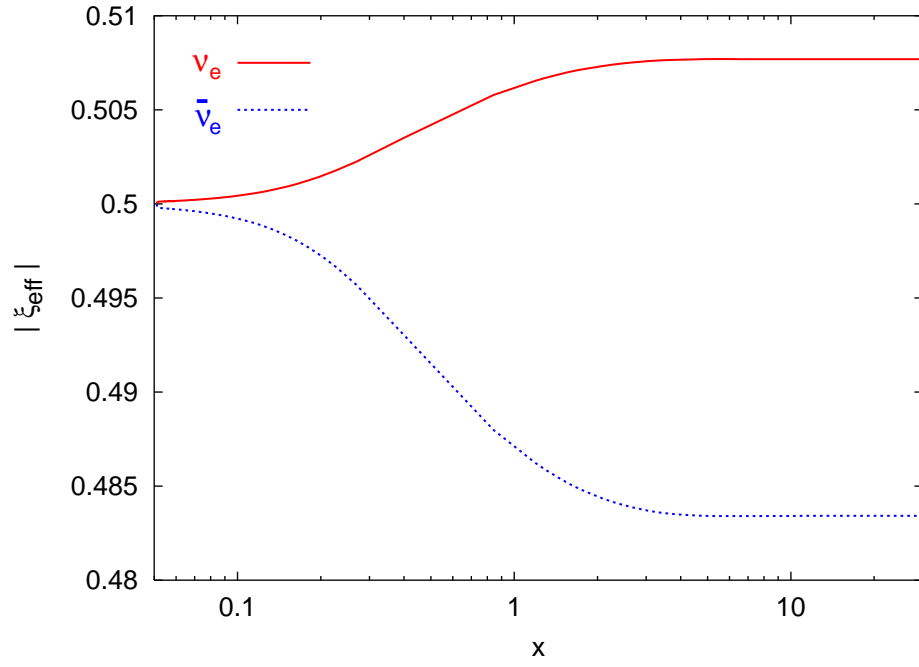


Figure 12: Evolution of the absolute value of the effective degeneracy parameter ξ (if the distribution function is written with an equilibrium form) for electron neutrinos and antineutrinos with momentum $y = 5$ ($\xi_e = 0.5, \xi_x = 1$).

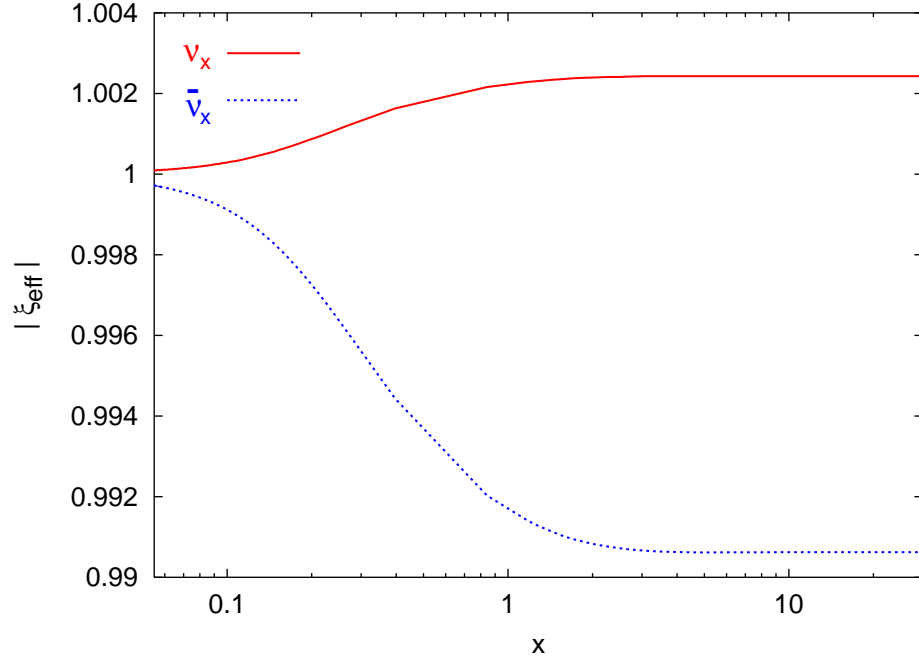


Figure 13: Same as previous figure, for muon or tau neutrinos and antineutrinos.

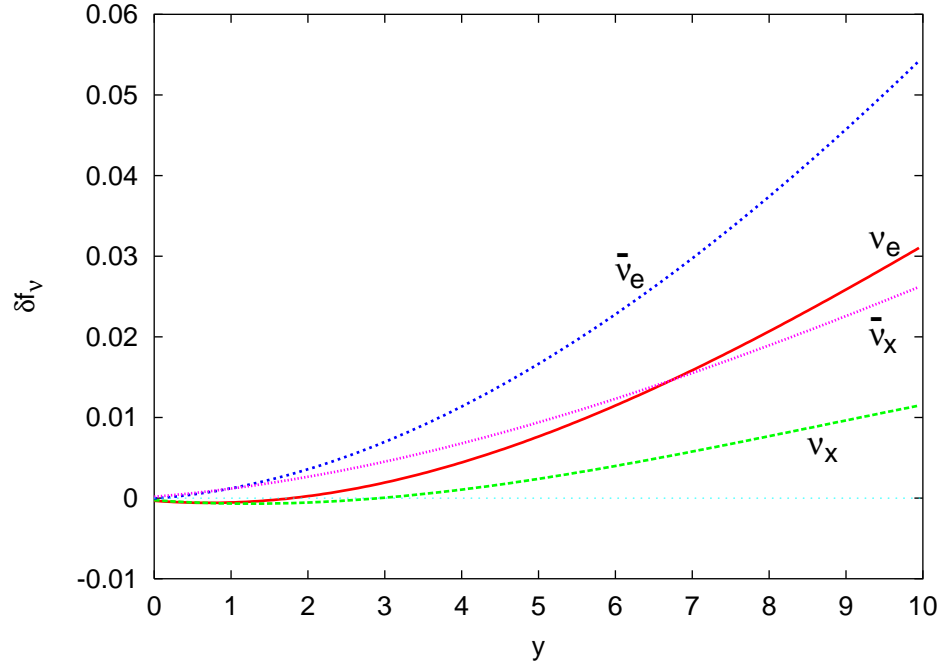


Figure 14: The final distortion as a function of momentum for the case $\xi_e = 0.5$ and $\xi_x = 1$.

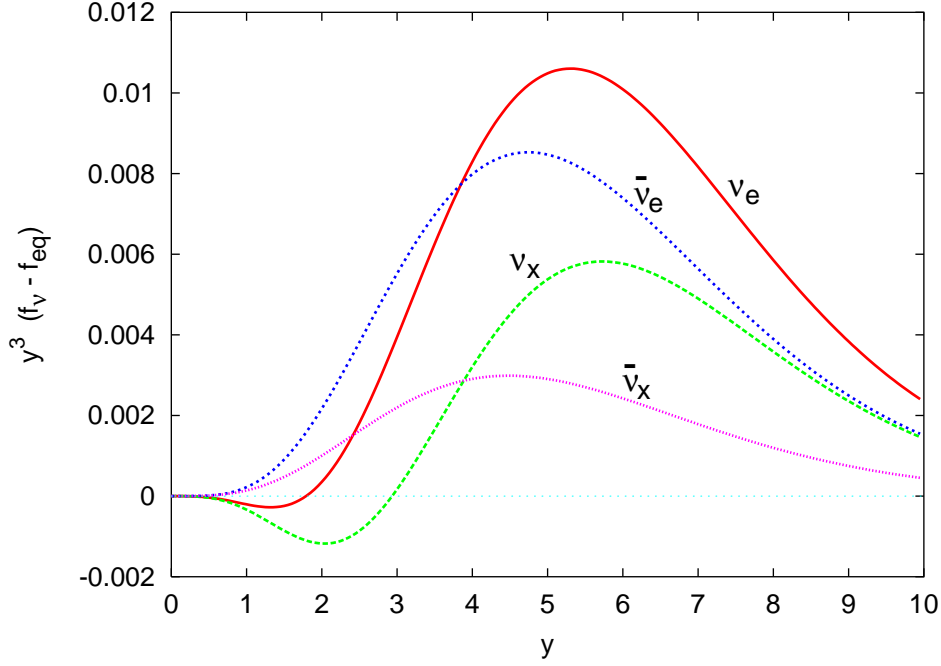


Figure 15: Final distortion of the differential energy density, as a function of momentum for the case $\xi_e = 0.5$ and $\xi_x = 1$.

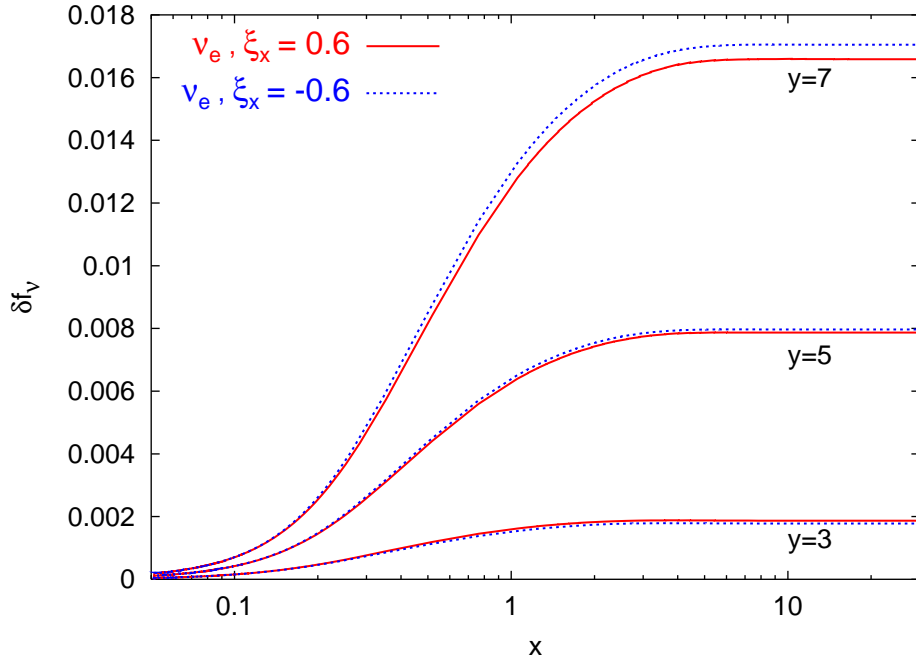


Figure 16: The evolution of δf_{ν_e} , as a function of x for $\xi_e = 0.5$, and $\xi_x = 0.6$ or $\xi_x = -0.6$, respectively.

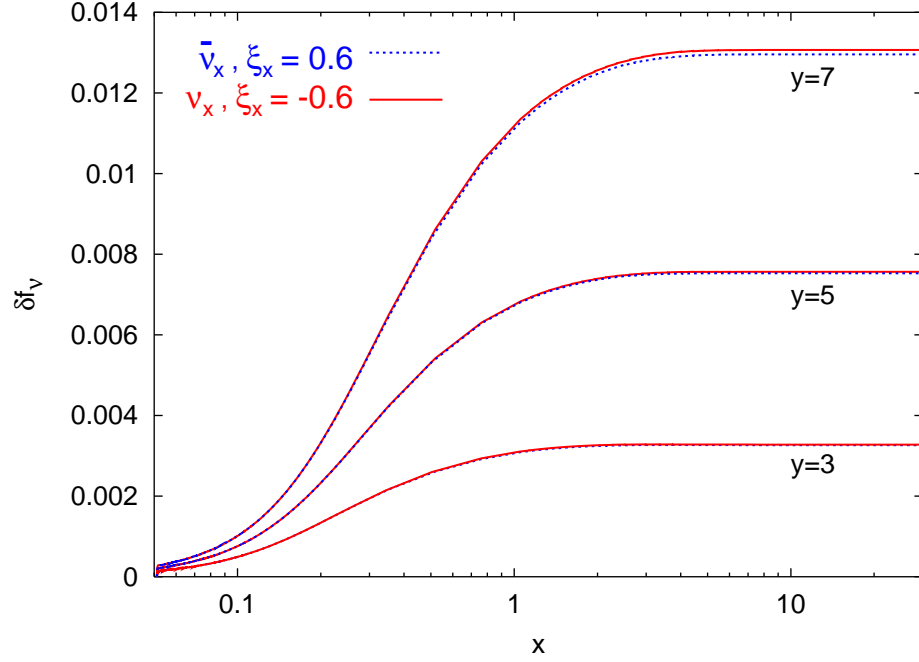


Figure 17: Same as previous figure for $\delta f_{\bar{\nu}_x}$ with $\xi_x = 0.6$ and δf_{ν_x} with $\xi_x = -0.6$.

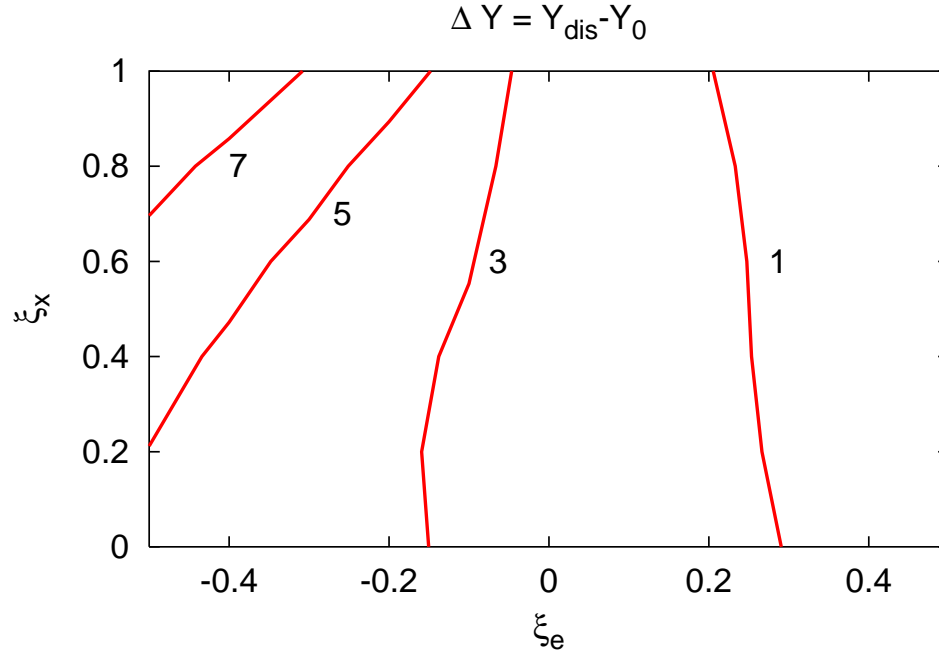


Figure 18: Effect of the neutrino distortion over the primordial abundance of ${}^4\text{He}$ as a function of the neutrino degeneracies ξ_e and ξ_x . The contours indicate equal values of ΔY in units 10^{-4} .

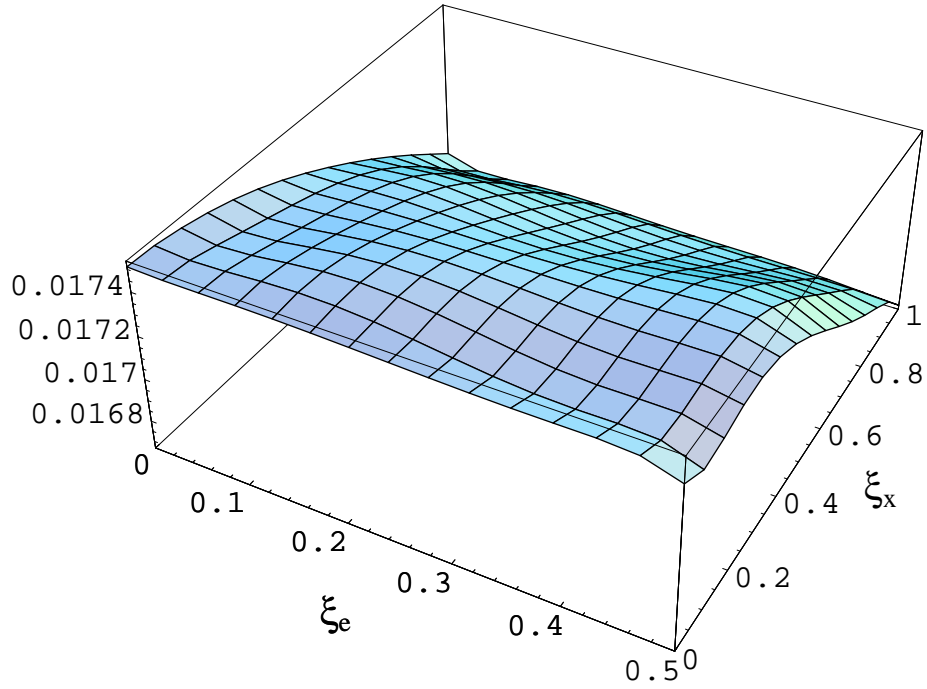


Figure 19: Effect of the neutrino distortion over the relic neutrino energy density, parameterized in terms of ΔN_ν , as a function of the neutrino degeneracies ξ_α .